

The ITO-capped WO₃ nanowires biosensor based on field-effect transistor in label-free protein sensing

Mohsen Shariati¹

Received: 21 December 2016 / Accepted: 20 April 2017 / Published online: 25 April 2017
© Springer-Verlag Berlin Heidelberg 2017

Abstract The fabrication of ITO-capped WO₃ nanowires associated with their bio-sensing properties in field-effect transistor diagnostics basis as a biosensor has been reported. The bio-sensing property for manipulated nanowires elucidated that the grown nanostructures were very sensitive to protein. The ITO-capped WO₃ nanowires biosensor showed an intensive bio-sensing activity against reliable protein. Polylysine strongly charged bio-molecule was applied as model system to demonstrate the implementation of materialized biosensor. The employed sensing mechanism was ‘label-free’ and depended on bio-molecule’s intrinsic charge. For nanowires synthesis, the vapor–liquid–solid mechanism was used. Nanowires were beyond a few hundred nanometers in lengths and around 15–20 nm in diameter, while the globe cap’s size on the nanowires was around 15–25 nm. The indium tin oxide (ITO) played as catalyst in nanofabrication for WO₃ nanowires growth and had outstanding role in bio-sensing especially for bio-molecule adherence. In applied electric field presence, the fabricated device showed the great potential to enhance medical diagnostics.

1 Introduction

In recent years, a wide range of protein and molecule biosensors have been designed and materialized that it outwits the request for the previous techniques such as fluorescence labeling and imaging [1–6].

The great interests have been developed to draw up and fabricate the label-free detector because of faster, lower-cost biosensor. By introducing new and novel detectors, the advanced biosensors would be more accessible to the medical societies. This approach is a critical step towards better diagnostics and specialized medical sciences [7]. In literature, the electronic detection of charge of molecule has been investigated; in there, it had been chosen the adsorption of poly(L-lysine) to the SiO₂ surface of the device. Poly(L-lysine) presents NH³⁺ groups at neutral pH that lead to an electrostatic attraction to glass and SiO₂. The thermodynamics of poly(L-lysine) adsorption from a liquid phase to a reactive glass surface has been investigated experimentally and theoretically [8].

For unlabeled sensing of the bio-molecules, detection mechanism uses the intrinsic protein physical properties. These physical properties include mass, polarizability, dielectric constant, electric charge, and electrical impedance [3]. By detection of bio-molecules, a signal will create by biosensors based on micromechanical oscillators [4]. The nanowire and nanotube field-effect transistors (FETs) can detect the charged bio-molecules [5, 6].

In the class of charge-sensitive biosensors, semiconducting metal oxides are extremely promising. Metal-oxide nanowires are one dimensional with a thin diameter of around 50–100 nm. All atoms of the metal-oxide nanowires are on the surface, carrier mobility is exceptionally high, and their sponsored lattice is extremely stable in biological environments [9].

It has recently been illustrated which some oxide nanostructures such as SiO₂ [10], TiO₂ [11, 12], ZrO₂ nanoparticles [13], MnO₂ [14], and Fe₃O₄ [15–17] would also be applied for the immobilization of protein to enhance the electron charge transfer between the immobilized protein and electrode.

✉ Mohsen Shariati
shariatimohsen59@gmail.com

¹ Institute for Nanoscience and Nanotechnology, Sharif University of Technology, 14588-89694 Tehran, Iran

Over the past decades, metal-oxide nanowires and nanorods have been the subject of intensive and wide interests for their outstanding structures, physical properties, and their requested potential applications [18–20]. Among them, In_2O_3 doped with tin, known as ITO metal oxide which is intensively used in electronics and optics industries and widely famed as a transparent conducting figure in optoelectronics technology [20–28]. Allocating to much larger surface areas prepared by ITO nanowires (NWs), it is amazing to evaluate them as the electrodes for organic LEDs and solar cells [19]. In recent years, much research efforts have been materialized on the exploiting of ITO nanocrystals, since they involve in extensive applications.

In this research, the fabrication of ITO (indium tin oxide) capped WO_3 nanowires, through the physical vapor deposition (PVD) mechanism and annealing associated with reactive and carrier gas atmosphere has been reported. In this route, first, the functionalized nanostructures have been fabricated. Then, they were applied for bio-sensing in label-free technique. The field-effect transistors measurements were used for the development of protocols for reliable protein sensing. The sensing method was relied only on the intrinsic charge of the bio-molecule. The strongly charged polylysine were used as sample for bio-sensing approach.

2 Experimental

For ITO-capped WO_3 nanowires fabrication, an easy method was used to form a self-assembled of the indium associated with tin films annealed in a horizontal tube furnace. The indium and tin metals precursor were sliced to small particles. Their size was around 0.3 mm in diameter and they put in a tungsten boat. For substrate cleansing, they put in an ultrasonic bath of acetone around 40 min; this process was followed by drying in N_2 gas flowing atmosphere. The deposition steps were followed, initially; the indium thin film in metallic formation was epitaxially formed on Si p-type substrates. This deposition was performed by a PVD mechanism (resistive evaporation deposition), under vacuum control. Then, tin and indium evaporated, respectively, and deposited on the first film for making sandwich-shaped film (indium + tin + indium). Figure 1 shows a schematic image of the applied PVD system. The deposition system (Thermal Evaporation, DTT model) was set up by the Nanostructured Coating Co. (Iran). The alumina boat was used to melt precursor. They evaporated to form the thin film. It is important to note that purity of indium and tin precursor metals was in 99.999% and their weight was 0.2 g. The ratio of In: Sn is 10–1. After (indium + tin) thin-film deposition process, the thin film

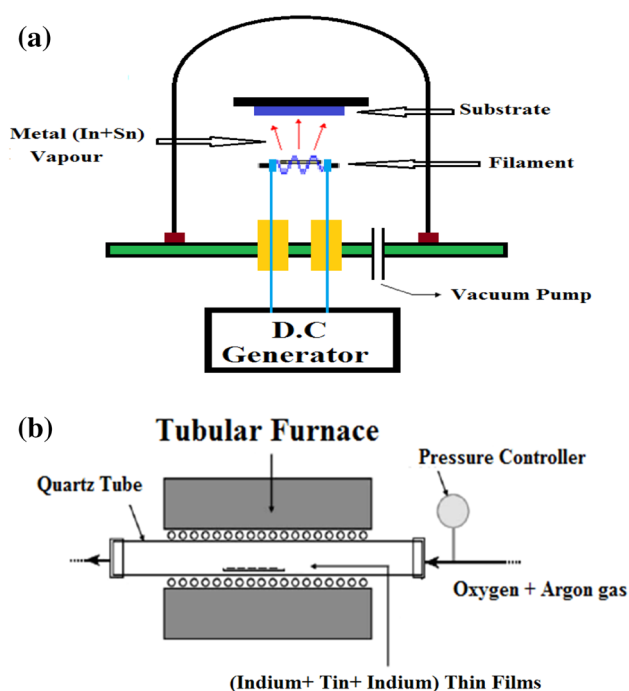


Fig. 1 Schematical pictures from deposition process. **a** Schematical illustration of resistive evaporation mechanism. **b** Tubular thermal evaporation furnace for annealing treatment

was put in the tubular furnace. In this step, tungsten metal was positioned in the tube associated with thin films and they were exposed to O_2 and Ar gas atmosphere presence. The under controlled pressure was kept in 10^{-2} mbar. In tubular furnace, temperature for sample was 1400°C . The outputs were characterized by different analysis measurements. For phase characterization, the X-ray diffraction spectrum (XRD) was applied. For morphology characterization, the field emission scanning electron microscope (FESEM) and a transmission electron microscopy (TEM and HRTEM) for exact measurements were applied. The XRD measurements were carried out using a Rigaku D/max RB X-ray diffractometer with $\text{CuK}\alpha$ line (40 kV, 100 mA). A Hitachi S-4160 field emission scanning electron microscope (FESEM) was used for characterization of the ITO nanostructures morphology. A transmission electron microscopy (TEM) (Philips, CM-30) was used to determine the morphology, sizes, and growth directions of the nanostructures (HRTEM and SAED patterns). Figure 2 shows the configuration of the bio-sensing setup schematically. The adsorption of the bio-molecules onto the ITO-capped WO_3 nanowires surface alters the surface state. To fabricate ITO-capped WO_3 nanowires FET device, the fabricated ITO-capped WO_3 nanowires were inserted in ethanol bath for 30 min, and then, the suspension (nanostructures included) was dropped onto the substrate (Si, p-type) with a SiO_2 nanoscale thin film on it (see Fig. 2). The Si substrate in high doping would play a role as a gate terminal to modulate

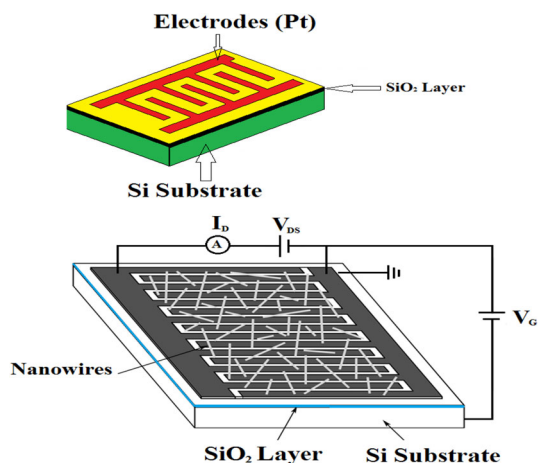


Fig. 2 Schematically fabricated ITO-capped WO₃ nanowires FET device. The *top* schematic picture is the device performing situation and *down* schematic picture is the device after ITO-capped WO₃ nanowires drop

the carrier density in the ITO-capped WO₃ nanowires. Source and drain electrodes with spacing of 2 μm were defined by the typical photolithography, this process was followed by resistive evaporation of Au (30 nm). After lift-off, the fabricated device was prepared for electrical transport measurements at room temperature with semiconductor parameter analyzer (HP-4155C).

3 Results and discussion

3.1 Morphological results

Figure 3 shows the typical FESEM images of the obtained products. In Fig. 3a, it reveals that the products consist of a large quantity of nanowires with globe cap on them. They are in typical lengths beyond a few hundred nanometers and diameter was around 15–20 nm, while the globe cap on the nanowires was around 15–25 nm. Figure 3a, b shows the sample nanostructures grown in one-directional growth mechanism. These results show that ITO catalyst exists and validate the catalyzed vapor–liquid–solid (VLS) growth mechanism. We can estimate that the indium tin oxide role as a catalyst helps structures to have such shapes and directly regulates the lateral side to grow in uniform, homogenous, and metrological shapes.

The fabricated nanowires demonstrated the highly defined ITO-capped WO₃ arrays. Figure 4 shows a cross-sectional FESEM picture of firstly indium + tin thin film which was utilized for ITO-capped WO₃ NWs arrays grown on Si substrate in physical vapor deposition. The thin film' thickness was about 3 μm . The surface of thin film was smooth and uniform. By further and additional techniques performing, the required process for nanowires

materializing has been achieved. The inset shows the final fabricated ITO-capped WO₃ nanowires and their related thickness. It is clearly seen that the regulated arrays were aligned on the Si substrate. In the inset, it is shown that the nanowires were around averagely 500 nm in length.

Figure 5 shows the TEM image of ITO-capped WO₃ nanowire from sample with a diameter dimension of ~ 20 nm in which their corresponding high-resolution TEM pictures are illustrated in inset. The HRTEM images indicate that the ITO-capped WO₃ nanowires are highly crystalline. However, the SnO₂ and In₂O₃ hetero-doping did not have prominent effect on nanowires growth. Obviously, there is no intense dislocation or cluster formation [23]. The HRTEM images confirm the morphology of the indium tin oxide-WO₃ heterostructure nanowires. The two inter-plane distances were measured, and the lattice planes as shown in Fig. 5 can be indexed to ITO (200) for globe cap with [111] the growth direction and (200) for nanowire with [040] the growth direction. The lattice spacing in sample for cap is 0.497 and 0.52 nm for nanowire. The mentioned lattice spacing of samples is coinciding to (200) and (200) planes. These crystal planes are consistent with In₂O₃ phase structure and WO₃. The growth direction which is consistent with the past articles was identified to be [111] for cap and [040] for nanowire [23].

Figure 6 shows the XRD pattern of the fabricated nanostructures. The room temperature measurement was carried out to evaluate the lattice phase structure of the synthesized nanostructures and their purity. The XRD spectrum was obtained for ITO-capped WO₃ nanowires at room temperature. The crystalline phases of ITO-capped WO₃ nanowires were confirmed. The XRD pattern shows the WO₃ main peaks which can be indexed to monoclinic phase in unit cell parameter $a = 0.7297$ nm, $b = 0.7539$ nm, $c = 0.7688$ nm, and $\beta = 90.91^\circ$ according to the JCPDS (43-1035), while the XRD pattern has peaks which can be well indexed to the body centered cubic structured In₂O₃ with the cell parameter $a = 10.12$ Å (JCPDS File No. 6-0416) [24–27]. The strong peaks indicate that the products are well crystallized. No impurity phases corresponding to other compounds can be detected. The XRD indicates that a mixture of tin doped In₂O₃ in globe cap shape on the WO₃ nanowires has been formed, which can be further conformed by the following analysis.

From Fig. 6, it is obviously clear that most of nanowires in sample were oriented to [111] (ITO cap) and [010] (NWs) direction, while a few of them directed in different orientations. This growth direction was proved by HRTEM measurement (Fig. 5). The growth factors affected on nanowires direction.

The main and prominent growth mechanism is catalyst accommodation process which is validated by external

Fig. 3 FESEM pictures of fabricated samples. As it is shown in **a** and **b**, there are one-dimensional structures in globe cap

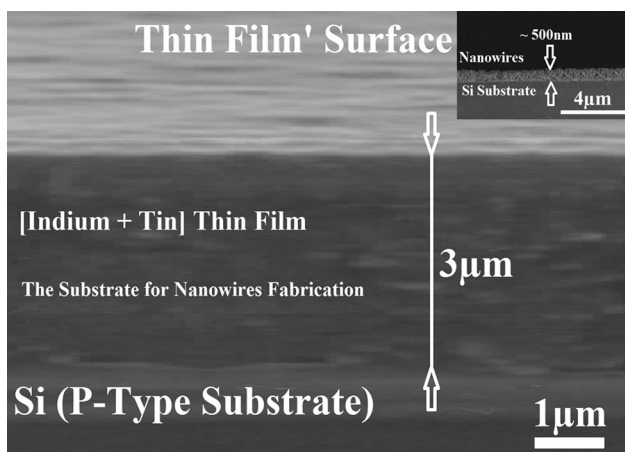
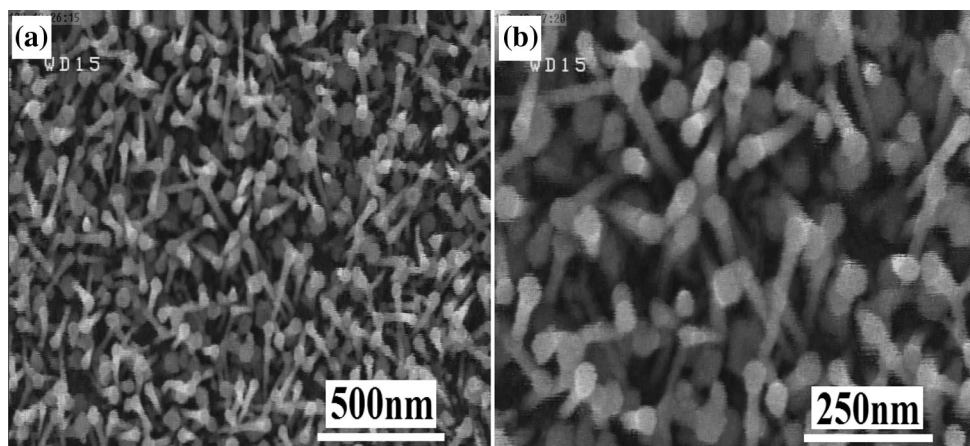


Fig. 4 Cross-sectional FESEM image of the first indium + tin thin film which was utilized for ITO-capped WO_3 NWs arrays grown on Si substrate. The inset shows the final fabricated ITO-capped WO_3 nanowires and their related thickness

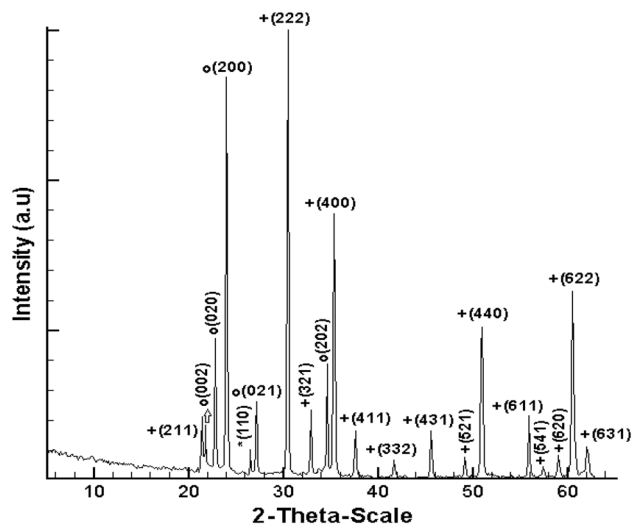


Fig. 6 XRD pattern of fabricated 1-D nanostructures (+: In_2O_3 , *: SnO_2 and o: WO_3) (right side). The sample is crystalline

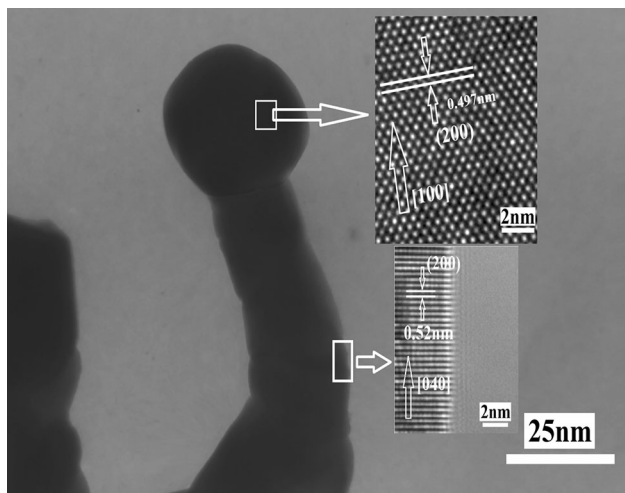


Fig. 5 Bright field transmission electron microscopy (TEM) images of ITO-capped WO_3 nanowires and the corresponding high-resolution TEM images of selected parts are shown

catalyst. In the present work, indium + tin + indium nanoparticle performs as a catalyst for nucleation in fabricating of nanowires.

3.2 Growth mechanism

The applied growth technique has provided the required meted factors to 1-D nanostructures growth. In this work, for achieving desired outcomes, the annealing process has ruled a key role for preparation nucleation sites. Most prominent and key one in materializing of the 1-D nanostructure is nucleation. In thermal evaporation mechanism, nucleation process hardly happens and few outcomes are emerged as 1-D nanostructures. It has to cite that the oxygen intensively helps the materialization of oxidized seeds, which provides nucleation sites for intended 1-D nanostructures growth in preferred direction. Oxidation process happened in nucleation stage on surface site which

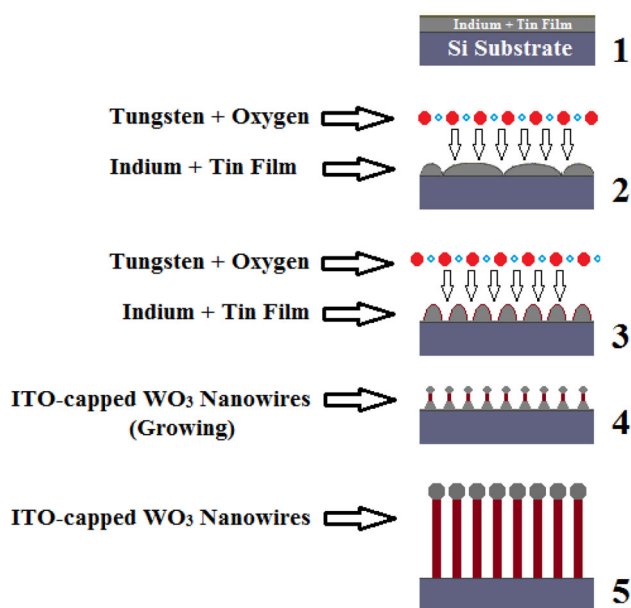


Fig. 7 Schematical growth process of the nanowires

decreases most of difficulties emerged in synthesis process especially in furnace setup [18–21, 23, 24].

The applied technique results to the 1-D nanostructures synthesis with interesting morphology. Laterally, the thinnest dimension of the nanowire is about 15 nm (Fig. 3). Then, WO₃ nanowires were found to nucleate from indium tin oxide-based nanoclusters. The lateral dimension of the nanowires precisely will be controlled by indium–tin alloy in ITO crystallization step. As a result, the lateral dimensions of the nanowires are thinner in comparison to the previous observed experiments. The growth mechanism of the fabricated indium–tin oxide-capped WO₃ nanowires in Fig. 3a and b is mainly due to two factors; the nucleated seeding in the substrate's nanoparticles and doping material. In the heat treatment, annealing process went on in gas atmosphere (argon + oxygen); the nanoscale sites prepared the needed conditions in preferred direction step in continuous growth. As the free energy was decreased, surface of nanocluster and nanoscale places were mainly absorbing sites for adsorbing nanoparticles and small molecules. As annealing temperature decreased, the lateral dimension of the 1-D nanostructures, especially morphology and structure phase, would cause to be out of control. The medium amount of the lateral dimension and height of the nanowires growth distribution on the seeded surface are related to annealing temperature [18–24].

Figure 7 shows schematically the nanowires growth process. They were fabricated through indium + tin thin film in controlled growth mechanism.

4 Bio-sensing analysis

The applied method shows important data from the ITO-capped WO₃ nanowires biosensor. The free carriers in the nanowires are holes and by positive ions or positive proteins were repelled. Depletion of free carriers causes a decrease in the conductance of the sensor. In this approach, conductance is altered by changing of the electrostatic potential V_g of the electrolyte solution that surrounds the sensor. In the applied measurements, the conductance changes due to proteins binding on the surface of the sensor. The total conductance change caused by protein binding can be expressed as an equivalent change in V_g .

4.1 Functionalization of nanowires

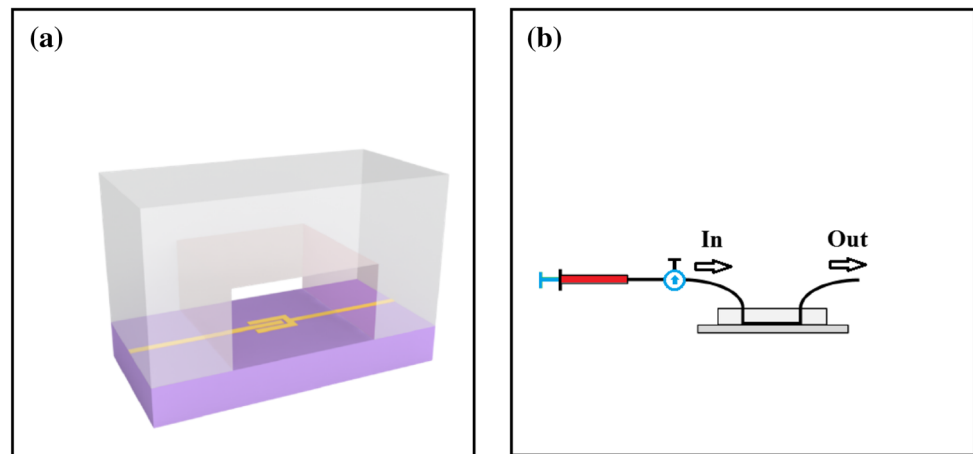
For functionalization of the ITO-capped nanowires to have strong bio-sensing, the binding site of bio-molecule and nanostructure should be materialized. In other mean must accept the interested molecule and reject others. Using the anti-bodies, the binding of the polylysine will be achieved. For the functionalization of the ITO-capped nanowires, it is followed a protocol developed by Ref. [9]. Initially, nanostructures were sonicated in ethanol bath. Then, they were incubated in a 1.5 mM purified solution of 1-pyrenebutanoic acid succinimidyl ester (PBASE) in DMF. They have been incubated at 7 h. Because of pyrene's ability to pi-stack on the nanowires surface, PBASE was chosen. The succinimidyl ester prepares a handle for bio-molecular conjugation. Then, it was degraded by hydro-photon mechanism. The DMF was dried by molecular sieves and kept in photo-free situation. Finally the device was dried in N₂ presence and rinsed in dry dimethylformamide (DMF). A drop of 1 mM ferritin (easy imaging in AFM and conjugation of primary amines to the succinimidyl ester) in PBS was deposited on the PBASE-modified nanowires and it was incubated for more 4 h.

4.2 Fluid delivery to the biosensor chip

For delivery, the solution of sample to the regulated area on the surface of nanowires in biosensor, micro-fluidic channels which were made from polydimethylsiloxane (PDMS) established. The channels materialize swift seals to the Si wafers which have been used for device fabrication.

Figure 8 shows the schematic picture of a PDMS channel (part A) on the nanowire field-effect transistor biosensor chip and the experiment set (part B). Fluid goes through from these channels. The magnified image shows the gap between electrodes and the width of the micro-fluidic channel. For creating a PDMS channel for fluid

Fig. 8 **a** Cross section of a PDMS channel (*gray*) on the metal-oxide nanowires FET biosensor chip (*purple*). Fluid is colored red for clarity. **b** Magnified image showing the gap between electrodes and the width of the micro-fluidic channel



flow, the mold was fabricated from 120 μm -thick photo-resist.

The mold patterned in a contact aligner was developed following the instrumental structure. The PDMS was mixed (10:1 ratio of resin to hardener) and then poured on top of the photo-resist mold. The PDMS is prepared in suitable time at room temperature and then removed from the mold. The materialized solution flow channels were 120 μm in tall and 240 μm in wide. The PDMS channel is pressed onto a nanowire transistor biosensor device to constitute a water-tight seal with the oxide surface. Using a home-made acrylic fixture, the PDMS was clamped in place. The fixture connects to inlet and outlet tubing and holds the Ag/AgCl reference electrode in contact with the solution in the channel. In nanowire device, a gold working electrode was used as a gate handling for the solution. The V_g measurements were obtained by the reference electrode.

4.3 Analyzing sensing data

By adsorbing the charged protein to the surface of the ITO-capped nanowire bio-FET sensor, there should be an electrostatic coupling between the protein and the ITO-capped WO_3 nanowires which relies on counter-ion screening and separation interval. The counter-ion screening is marked by the Debye length [29–31].

The ITO-capped WO_3 nanowires bio-FET sensor's response exponentially will deteriorate with separation interval. The exponential decay constant is λ_D . In our experiment, we simulate the biological conditions. We were used the PBS with $\lambda_D \sim 1$ nm, 137 mM for NaCl, and 10 mM for $\text{Na}_3(\text{PO}_4)$, so the separation interval should be ~ 1 nm for optimized sensing [29–31]. The functionalization arrangements typically exploit anti-bodies to grip precisely the target bio-molecules from the solution. The anti-body operates as 10–15 nm spacer between the nanowire and the bio-molecular target. Therefore, bio-

sensing in biological circumstances for the mentioned mechanism ($\lambda_D \sim 1$ nm) is not practical [29–31]. An alternative outlook to the matter of electrostatic screening is to decrease the size of the functionalized bio-molecule on the surface of the bio-FET sensor. That outlook brings an anti-interference ability for bio-FET sensor. The electrostatic coupling through size effect between the nanowires and bio-molecule creates a physical bond to clear the other jeopardizing parameters.

There are several technical improvements which illustrate the importance of size effects and justify the development of nanoscale FET biosensors. First, biological recognition at the sensor surface is reflective of the entirety of the physical signal across the whole sensor device [32]. Thus, the sensitivity of the device, relating to its signal-to-noise ratio is improved by increasing the surface-to-volume ratio. Whereas attachment of a bio-molecule to a macro-scale planar device affects the “surface” characteristics, attachment to a nanoscale wire affects the “bulk” characteristics [32]. Second, many of the biological molecules of interest in bio-medical, environmental, and food applications are known to have sizes on the micro- or nanoscale. Thus, a device with submicron or nanoscale dimensions will have the best efficiency as a biological sensor [32]. Third, as the device size is reduced to the nanoscale, properties such as the mobility of the charge carrier change finite size effects dominate the device character, and nanodevice performance is enhanced [32].

However, some researchers have answered this matter by utilizing low-salt buffers. In addition to annexing an extra sample preparation pace, the utilization of low-salt buffers will decrease the affinity of anti-body-antigen binding. Low-salt concentrations can also lead to weak pH buffering [29–31].

Figure 9 illustrates the sensing experiment that tests bio-molecule with intrinsic charge; polylysine (a protein with at pH 7.4, one positive charge per monomer). In Fig. 9, it is

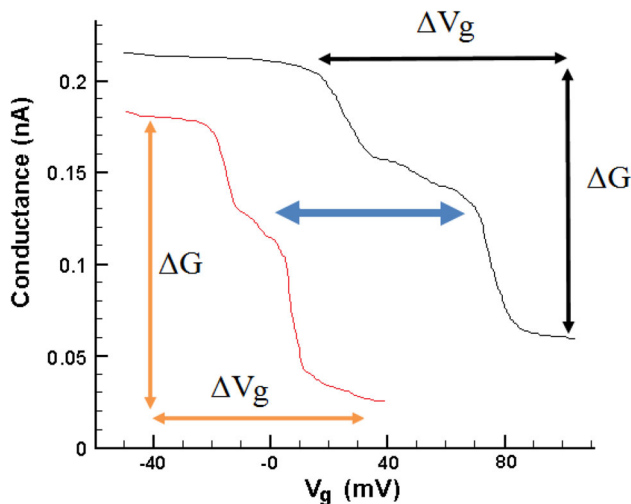


Fig. 9 ITO-capped WO₃ nanowires biosensor measurements. Transistor curve (conductance vs. V_g) of sensor gated by an electrolyte solution. ΔG and ΔV_g illustrate the effect of polylysine absorption. Biosensor signals depend on the charge of the bio-molecule. Transistor curves measured before (black) and after (red) polylysine binding. In this graph, it is seen the voltage shift for gate voltage was +91 mV to left, the changes ΔV_g (70 mV); conductance ΔG (0.16 nA) after polylysine binding and ΔV_g (85 mV); conductance ΔG (0.14 nA) before polylysine binding, respectively

seen that polylysine electrostatic binding is equal to a shift in gate voltage $\Delta V_g = +91$ mV. From Fig. 9, the sign of ΔV_g is related to the polarity of the tested biological molecules that is the main source of bio-molecule diagnostics. The graph's gradient in Fig. 9 for before and after polylysine binding shows after polylysine binding that the gradient was intensive than before. Fluorescence imaging reveals that polylysine binds to all bare silicon oxide surfaces [28]. The main force in binding between semiconductor ITO-WO₃ nanowires and polylysine (positive charge) was coulomb's potential force interaction.

Previously, it is noted that the biosensor responses are mainly depended on the bio-molecule's charge. In Fig. 9, the measured field-effect transistor graph (conductance vs. gate voltage) of biosensor which gated by an electrolyte solution is shown. ΔG and ΔV_g illustrate the effect of polylysine absorption as conductance against gate voltage. The FET response curves measured before (black) and after (red) polylysine binding. In this graph, it is shown that the voltage shift for gate voltage was +91 mV to left, the changes ΔV_g (70 mV); conductance ΔG (0.16 nA) after polylysine binding and ΔV_g (85 mV); conductance ΔG (0.14 nA) before polylysine binding.

For comparison ΔV_g because of polylysine bio-molecule binding to the previous theoretical approximated estimations, using the Gouy–Chapman Stern model, it is estimated that there is a binding by a layer of cations to the negative charge, semiconductor ITO-WO₃ nanowires

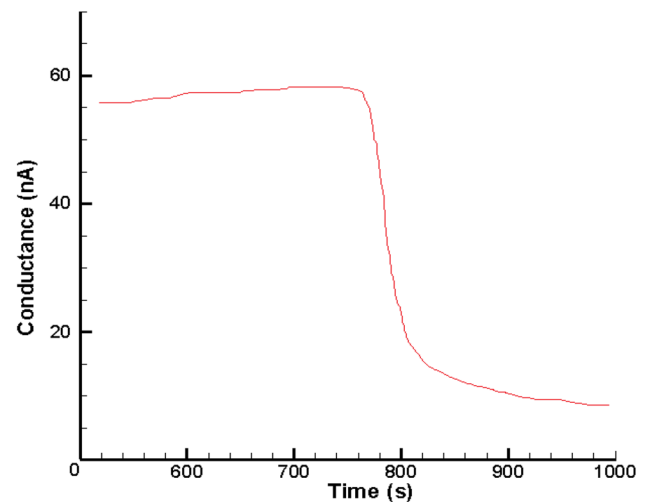


Fig. 10 Conductivity of nanowires changes. This change was due to polylysine binding on the surface of the biosensor. The real-time bio-sensing, V_g fixed in 80 mV, informs the polylysine biochemical binding on the surface of the nanowire in biosensor

surface (the Stern layer should be around 1 nm). A layer of accumulated examining ions diffuses into the sample solution. By diffusing the layer, the highest energy difference of nearly around 100 mV would be maintained. The ITO nanoparticles and WO₃ nanowires are in range of around a few nanometers, and therefore, the most of the ITO-capped WO₃ nanowires settle in diffusing layer that ΔV_g is confined to 100 mV. This matches with the performed experiment in which the maximum voltage shift for polylysine was +91 mV.

In Fig. 10, the conductivity of nanowires changes in time duration. This change was due to polylysine binding on the surface of the biosensor. In Fig. 10, the real-time bio-sensing, V_g fixed in 80 mV, informs the polylysine biochemical binding on the surface of the nanowire in biosensor. 25 $\mu\text{g/ml}$ of protein submerged in phosphate buffered saline was injected at 780 s, in 4 ml/h flow rate.

5 Conclusions

In this paper, the ITO (indium–tin oxide)-capped WO₃ nanowires by physical vapor deposition growth mechanism with annealing technique in reactive and carrier gas presence have been fabricated. In this approach, by fabrication of functionalized nanostructures, they were applied for protein sensing in label-free technique. The field-effect transistors setup was used for the development of protocols for bio-sensing. The sensing method was relied only on the intrinsic charge of the bio-molecule. The strongly charged polylysine were used as sample for bio-sensing approach. The applied method for bio-sensing demonstrated the

intensive and reliable response. This label-free mechanism will be widely used in medical diagnostics.

Compliance with ethical standards

Human and animal rights This article does not contain any studies with human or animals subjects performed by author.

Funding There are currently no funding sources in this article.

Conflict of interest The author declares that he has no conflict of interest.

References

1. J. Homola, Present and future of surface plasmon resonance biosensors. *Anal. Bioanal. Chem.* **377**, 528 (2003)
2. R. Yan, S. Mestas, G. Yuan, R. Safaisini, D. Dandy, K. Lear, Label-free silicon photonic biosensor system with integrated detector array. *Lab Chip* **9**, 2163 (2009)
3. S. Daniels, N. Pourmand, Label-free impedance biosensors: opportunities and challenges. *Electroanalysis* **19**, 1239 (2007)
4. P.S. Waggoner, H.G. Craighead, Micro- and nanomechanical sensors for environmental, chemical, and biological detection. *Lab Chip* **7**, 1238 (2007)
5. F. Patolsky, G. Zheng, C.M. Lieber, Nanowire-based biosensors. *Anal. Chem.* **78**, 4260 (2006)
6. B.L. Allen, P.D. Kichambare, A. Star, Carbon nanotube field-effect-transistor-based biosensors. *Adv. Mater.* **19**, 1439 (2007)
7. J.R. Heath, M.E. Davis, L. Hood, Nanomedicine-revolutionizing the fight against cancer. *Scientific American* (2009)
8. F. Pouthas, C. Gentil, D. Côte, G. Zeck, B. Straub, U. Bockelmann, *Phys. Rev. E* **70**, 031906 (2004)
9. B. Liu, J. Liu, DNA adsorption by indium tin oxide nanoparticles. *Langmuir* **31**, 371 (2015)
10. P. He, N. Hu, J.F. Rusling, Driving forces for layer-by-layer self assembly of films of SiO nanoparticles and heme proteins. *Langmuir* **20**, 722 (2004)
11. A. Viticoli, A. Curulli, A. Cusma, S. Kaciulis, S. Nunziante, L. Pandolfi, F. Valentini, G. Padeletti, Third-generation biosensors based on TiO nanostructured films. *Mater. Sci. Eng. C-Biomet. Supramol. Syst.* **26**, 947 (2006)
12. A.H. Liu, M.D. Wei, I. Honma, H.S. Zhou, Direct electrochemistry of myoglobin in titanate nanotubes film. *Anal. Chem.* **77**, 8068 (2005)
13. S.Q. Liu, Z.H. Dai, H.Y. Chen, H.X. Ju, Immobilization of hemoglobin on zirconium dioxide nanoparticles for preparation of a novel hydrogen peroxide biosensor. *Biosens. Bioelectron.* **19**, 963 (2004)
14. Y. Lvov, B. Munge, O. Giraldo, I. Ichinose, S.L. Suib, J.F. Rusling, Films of manganese oxide nanoparticles with polycations or myoglobin from alternate-layer adsorption. *Langmuir* **16**, 8850 (2000)
15. E. Katz, O. Lioubashevski, I. Willner, Magnetic field effects on cytochrome c-mediated bioelectrocatalytic transformations. *J. Am. Chem. Soc.* **126**, 11088 (2004)
16. G. Zhao, J.J. Xu, H.Y. Chen, Fabrication, characterization of FeO multilayer film and its application in promoting direct electron transfer of hemoglobin. *Electrochem. Commun.* **8**, 148 (2006)
17. E. Katz, I. Willner, Switching of directions of bioelectrocatalytic currents and photocurrents at electrode surfaces by using hydrophobic magnetic nanoparticles. *Angew. Chem. Int. Edit.* **44**, 4791 (2005)
18. M. Shariati, M. Darjani, The lateral In₂O₃ nanowires and pyramid networks manipulation by controlled substrate surface energy in annealing evolution. *J. Cryst. Growth.* **436**, 104–112 (2016)
19. Y.Y. Kee et al., Low-temperature synthesis of indium tin oxide nanowires as the transparent electrodes for organic light emitting device. *Nanotechnology.* **23**, 025706 (2012)
20. M. Shariati, S. Alishavandi, Phototransistor properties of indium tin oxide nanowires grown by RF sputtering mechanism and annealing process. *NANO* **10**(01), 1550006 (2015)
21. W.C. Chang, C.H. Kuo, C.C. Juan, P.J. Lee, Y.L. Chueh, S.J. Lin, Sn-doped In₂O₃ nanowires: enhancement of electrical field emission by a selective area growth. *Nanoscale Res. Lett.* **7**, 684 (2012)
22. Q. Wan et al., Vertically aligned tin-doped indium oxide nanowire arrays: epitaxial growth and electron field emission properties. *Appl. Phys. Lett.* **89**, 123102 (2006)
23. M. Shariati, The continuous and persistent periodical growth induced by substrate accommodation in In₂O₃ nanostructure chains and their photoluminescence properties. *Appl. Phys. A* **118**, 997 (2015)
24. M. Shariati, The indium oxide micro and nanopyramids: morphology materializing and H₂S sensing properties. *Int. J. Mod. Phys. B* **29**(20), 1550144 (2015)
25. P. Nguyen et al., Direct integration of metal oxide nanowire in vertical field-effect transistor. *Nano Lett.* **4**, 651 (2004)
26. X.S. Peng et al., Large-scale synthesis of In₂O₃ nanowires. *Appl. Phys. A* **74**, 437 (2002)
27. S.M. Karadeniz, A.E. Ekinci, D. Tatar, M. Ertuğrul, XRD and SEM results of WO₃ thin films deposited on quartz glasses. *Int. J. Appl. Sci. Technol.* **4**, 136 (2014)
28. X. Yang, Q. Zhang, Y. Sun, S. Liu, Direct electron transfer reactivity of glucose oxidase on electrodes modified with zirconium dioxide nanoparticles. *IEEE Sens. J.* **7**, 1735 (2007)
29. E. Stern, R. Wagner, F.J. Sigworth, R. Breaker, T.M. Fahmy, M.A. Reed, Importance of the Debye screening length on nanowire field effect transistor sensors. *Nano Lett.* **7**, 3405 (2007)
30. G. Zheng, F. Patolsky, Y. Cui, W.U. Wang, C.M. Lieber, Multiplexed electrical detection of cancer markers with nanowire sensor arrays. *Nat Biotech* **23**, 1294 (2005)
31. K. Maehashi, T. Katsura, K. Kerman, Y. Takamura, K. Matsumoto, E. Tamiya, Label-free protein biosensor based on Aptamer-modified carbon nanotube field-effect transistors. *Anal. Chem.* **79**, 782 (2006)
32. N. Elfstrom, R. Juhasz, I. Sychugov, T. Engfeldt, A.E. Karlstrom, J. Linnros, Surface charge sensitivity of silicon nanowires: size dependence. *Nano Lett.* **7**, 2608 (2007)